Generation of Terahertz Superimposed Perfect Vortex Beams

Yongqiang Yang, Tianyi Wang, Kejia Wang, Zhengang Yang, and Jinsong Liu

***Abstract*—A terahertz (THz) superimposed perfect vortex (SPV) beam is generated by using a designed superimposed optimal phase element (SOPE) at 0.3 THz. As the superimposed topological charge changes, the ring radius of THz SPV beams remains almost constant in the experiment, whose relative error is only 0.96%. The perfect vortex property is confirmed. The intensity profile of THz SPV beams is a ring with equally spaced breakpoints. The superimposed topological charge carried can be judged directly by identifying the number of breakpoints. The ring radius is linearly related to the radial wave vector, which can be adjusted. Such THz SPV beams have promising applications for THz fiber communication systems based on vortex beams.**

***Index Terms*—Terahertz, vortex beam, perfect vortex beam, diffractive elements.**

I. Introduction

TERAHERTZ (THz) wave, whose frequency range between microwave and infrared light wave, has the ability to provide large bandwidth and realize Tbps data rate transmission [1], [2]. Vortex beams with helical phase structures have attracted a lot of attention [3]. Optical vortex beams have been widely applied in communication systems, both in free space [4] and fiber [5], [6], because of the orbital angular momentum (OAM) carried [7]. THz vortex beams go beyond conventional THz waves, which will promisingly achieve ultrahigh data capacity and speed based on THz communication systems [8]. The transmission of the THz vortex beams in free space is easily affected by atmospheric turbulence. A fiber capable of stably transmitting the THz vortex beams is required. Currently, research on the fiber for transmitting the THz vortex beams has emerged [9]–[11]. However, the ring radius of THz vortex beams is continually larger as the topological charge increases. Vortex beams with multiple topological charges will be a challenge to couple into a fixed-aperture fiber.

Fortunately, Ostrovsky *et al.* [12] created a new beam, called perfect vortex (PV) beam, whose ring radius is independent of its topological charge. This property is called as the perfect vortex property. These PV beams already have some special applications in microparticle trapping [13], optical communication [14], [15], and quantum optic [16]. Currently, the research related to PV beams is mainly in the optical domain [17]. There are few reports in the THz domain. Recently, an optimal phase element (OPE) is employed to generate a THz PV beam at 0.1 THz [18]. However, there are some disadvantages accompanying the THz PV beam. On the one hand, the intensity profile of THz PV beams is theoretically uniform along the angular direction, which will make it not possible to determine the topological charge directly from the intensity profile. A device to detect the topological charge is necessary at the receiving end, which will complicate the transmission system of THz PV beams. On the other hand, as the topological charge changes, the ring radius of THz PV beams remains constant in theory but varies considerably in the experiment. This variation will reduce the coupling efficiency of the fiber communication systems based on THz PV beams.

In this paper, we generated a THz superimposed perfect vortex (SPV) beam by using a superimposed optimal phase element (SOPE). The SOPE is specially designed. The perfect vortex property and variation of ring radius with radial wave vector are investigated. The experimental results show that the ring radius of THz SPV beams is nearly fixed as the superimposed topological charge changes, whose relative error is very small. The intensity profile of THz SPV beams is a ring with equally spaced breakpoints. The superimposed topological charge carried can be determined directly. The ring radius is linearly related to the radial wave vector, which can be adjusted. The THz SPV beams may be more suitable for THz fiber communication systems than the THz PV beams.

II. Design

In previous work, OPEs have been employed to generate THz PV beams [18], [19]. However, the ring radius of THz PV beams varies considerably as the topological charge changes in the experiment. This variation may be caused by the scattering of the complex OPEs. Moreover, fabricating OPEs with complex phase profiles is difficult. Although these diffractive elements can be easily fabricated by 3D printing technology [20], [21], it is a challenge for other machining techniques. To simplify the diffractive element and then obtain a THz vortex beam whose ring radius does not vary with topological charge, a SOPE is specially designed. The SOPE is a superposition of two OPEs with the same value and opposite sign topological charge. A THz

Manuscript received May 26, 2021; revised July 8, 2021; accepted July 21, 2021. Date of publication July 26, 2021; date of current version August 6, 2021. This work was supported by the National Natural Science Foundation of China under Grant 11574105. *(Corresponding author: Jinsong Liu.)*

Yongqiang Yang, Tianyi Wang, Kejia Wang, and Jinsong Liu are with the Wuhan National Laboratory for Optoelectronics, Huazhong University of Science and Technology, Wuhan 430074, China (e-mail: yqyanghust@gmail.com; tianyiwang@vip.163.com; wkjtode@sina.com; jsliu4508@vip.sina.com).

Zhengang Yang is with the School of Optical and Electronic Information, Huazhong University of Science and Technology, Wuhan 430074, China (e-mail: mikleyang@163.com).

Digital Object Identifier 10.1109/JPHOT.2021.3099843

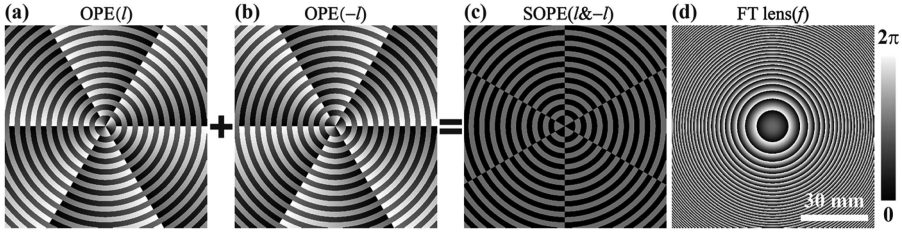

Fig. 1. Generation process of a SOPE. (a) and (b) OPEs. (c) SOPE. (d) FT lens.

Gaussian beam passes through a SOPE and a Fourier transform (FT) lens. The SOPE constructs the superimposed optimal phase mask. The FT lens performs the FT. A THz SPV beam is created at the back focal plane of the FT lens. So it can be stated that the THz SPV beam is also a superposition of two THz PV beams with the same value and opposite sign topological charge. This superposition will cause some phase jump of the THz SPV beam along the angular direction, resulting in a ring beam with equally spaced breakpoints.

Superposing transmission function of two OPEs with topological charges of l and $-l$, the superimposed transmission function can be expressed as

$$U_1(r,\theta) = \mathrm{sgn}[J_l(\alpha r)]\exp(il\theta) + (-1)^l \mathrm{sgn} \times [J_{-l}(\alpha r)]\exp(-il\theta) \quad (1)$$

with (r,θ) the polar coordinates in the plane of the OPE, sgn(x) the signum function, α the radial wave vector and J_l the l^{th} order Bessel function of the first kind. The $(-1)^l$ denotes a phase shift between two OPEs. Due to $\mathrm{sgn}[J_{-l}(\alpha r)] = (-1)^l\,\mathrm{sgn}[J_l(\alpha r)]$, the superimposed transmission function can be simplified as

$$\begin{aligned} U_1(r,\theta) &= \mathrm{sgn}\left[J_l(\alpha r)\right]\left[\exp(il\theta) + \exp(-il\theta)\right] \\ &= 2\mathrm{sgn}\left[J_l(\alpha r)\right]\cos(l\theta). \end{aligned} \quad (2)$$

It is obvious that the transmission function of superimposed two OPEs is a series of real numbers. Then, the phase profile of superimposed two OPEs can be expressed as

$$\Psi_1(r,\theta) = \begin{cases} 0, & 2\mathrm{sgn}[J_l(\alpha r)]\cos(l\theta) > 0, \\ \text{any}, & 2\mathrm{sgn}[J_l(\alpha r)]\cos(l\theta) = 0, \\ \pi, & 2\mathrm{sgn}[J_l(\alpha r)]\cos(l\theta) < 0. \end{cases} \quad (3)$$

The phase profile is the phase hologram of superimposed two OPEs, which form the diffractive phase element, namely the SOPE. Hence, the SOPE is a superposition of two OPEs. Figs. 1(a)–1(c) illustrate the generation process of a SOPE. Compared to two OPEs, the SOPE is simple, whose phase contains two main values, namely 0 and π. The SOPE is similar to the zone phase plate [22]. The topological charge carried by SOPEs is called the superimposed topological charge, which is written as $l_s = +l\&{-}l$.

Generally, a focal lens can act as an FT lens, whose transmission function and phase profile can be expressed as, respectively,

$$U_2(r,\theta) = \exp\left[-\frac{ik_0 r^2}{2f}\right], \quad (4)$$

$$\Psi_2(r,\theta) = -\frac{k_0 r^2}{2f}. \quad (5)$$

Here, $k_0 = 2\pi/\lambda$ is the wavenumber in free space, λ is the wavelength, f is the focal length of the FT lens. The phase profile of the FT lens is shown in Fig. 1(d).

According to the equivalency of optical path, the height profiles of the SOPE and FT lens from the phase profiles of Eq. (3) and Eq. (5) can be calculated as, respectively,

$$h_1(r,\theta) = \frac{\lambda}{2\pi(n-1)}\mathrm{mod}[\Psi_1(r,\theta), 2\pi] + h_0, \quad (6)$$

$$h_2(r,\theta) = \frac{\lambda}{2\pi(n-1)}\mathrm{mod}[\Psi_2(r,\theta), 2\pi] + h_0 \quad (7)$$

with n the material refractive index. The mod[Ψ,2π] denotes that Ψ is wrapped modulo 2π, which is to reduce the material absorption. The $h_0 = 1.5$ mm is the base plate thickness, which can support the physical structure. The 3D models of the SOPEs and FT lens can be created by the height profiles.

III. Experimental Setup and Fabrication

Fig. 2 schematically illustrates the experimental setup for generating THz SPV beams. A multiplier-chain (Virginia Diode Inc., Charlottesville, VA, USA) driven by a Gunn diode (Spacek Lab Inc., Santa Barbara, CA, USA) acts as a source with the output power 0.3 mW, which radiates THz continuous waves with a frequency of 0.3 THz. The THz continuous waves are transmitted into free space via a WR-3.4 diagonal horn antenna. A high-density polyethylene lens acts as a collimating lens (CL) to collimate the diverging THz beam. The collimated beam has a diameter $2w_0 = 24.32$ mm, whose normalized intensity profile is shown in Fig. 2(a). A SOPE is employed to modulate the phase of the collimated beam. A Fourier transform is then performed by placing an FT lens behind the SOPE. In theory, a THz SPV beam will be generated at the back focal plane of the FT lens. An experimental intensity profile of the THz SPV beam with $l_s = +3\&{-}3$ is shown in Fig. 2(b). A THz ultra-broadband detector (Gamma Technologies Inc., Shanghai, China) can be utilized for receiving the THz waves, where a lock-in amplifier (SR830, Stanford Research Systems, Sunnyvale, CA, USA) is connected to a chopper for amplifying the dynamic range of the THz signal. A three-axis translation stage drives the detector for 3D scanning. In the xy-plane, the detection area and sampling interval are 90 mm×90 mm and 0.5 mm, respectively.

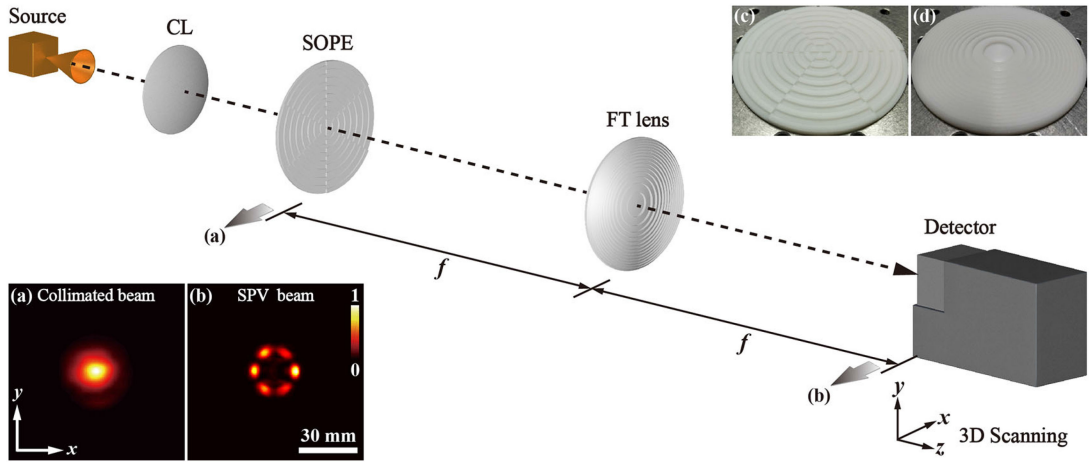

Fig. 2. Schematic of the experimental setup for generating the THz SPV beams. (a) Collimated beam. (b) SPV beam. (c) SOPE. (d) FT lens.

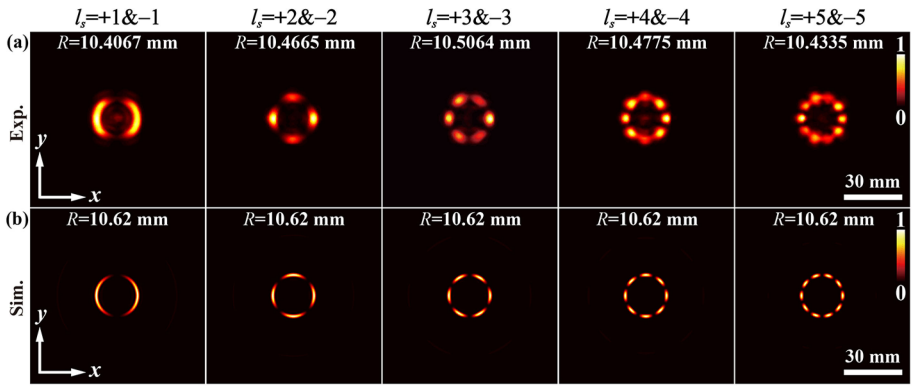

Fig. 3. (a) Experimental and (b) simulated intensity profiles of THz SPV beams with different superimposed topological charges.

The height profile of SOPEs is mainly composed of two values. The SOPEs can be manufactured using some simple techniques, such as Machine Polishing [23]. Recently, a variety of terahertz structured beams have been generated by the diffractive elements fabricated by 3D printing technology [24], [25] and liquid crystal polymer [26]. The 3D printing technique is quick and cost-efficient. In this study, the SOPEs and FT lens are fabricated from the created 3D models by 3D printing technology. The 3D printing material selected is a photosensitive resin, whose refractive index and absorption are 1.61 and 1.35 mm^{-1} in 0.3 THz, respectively. Figs. 2(c) and 2(d) show the pictures of the fabricated SOPE and FT lens, respectively. Here, the superimposed topological charge $l_s = +3\&–3$, the radial wave vector $\alpha = 1.339$ mm^{-1}, the focal length $f = 50$ mm. These elements all have a diameter of 76.2 mm. The maximum heights of the SOPE and FT lens are 2.319 mm and 3.138 mm, respectively.

IV. Results and Discussions

To verify the perfect vortex property, THz SPV beams with different superimposed topological charges are generated experimentally at the back focal plane of the FT lens ($f = 50$ mm). Fig. 3(a) shows the normalized intensity profiles. For the SOPEs, the superimposed topological charge l_s ranges from +1&–1 to +5&–5, the radial wave vector $\alpha = 1.339$ mm^{-1}. Intuitionally, the intensity profile of THz SPV beams is a ring with equally spaced breakpoints. These breakpoints are the result of phase jumps, whose number is equal to $2|l|$. As the superimposed topological charge changes, the ring radius remains almost constant. Meanwhile, the ring radius of THz SPV beams is computed by fitting the intensity profile. We assume that the fitting formula for these intensity profiles is $I(x, y) = A_0 \exp[(\sqrt{x^2 + y^2} - R)^{2/w^2}]$. The optimal parameters including the intensity scale factor A_0, ring radius R, and ring width w. Using the least-squares criterion, the fitted ring radius is marked in the intensity patterns. As can be seen from the fitted results, the ring radius remains almost constant, which only has some very slight differences appearing in the experiment. The relative error of the maximum and minimum of the ring radius is only 0.96%, which is very small. In the experiment, this very small relative error will increase the coupling efficiency of the fiber communication systems based on THz SPV beams. The numerically simulated results based on the angular spectrum [27] are shown in Fig. 3(b), which has the same experimental parameters. The simulated intensity profile of THz SPV beams

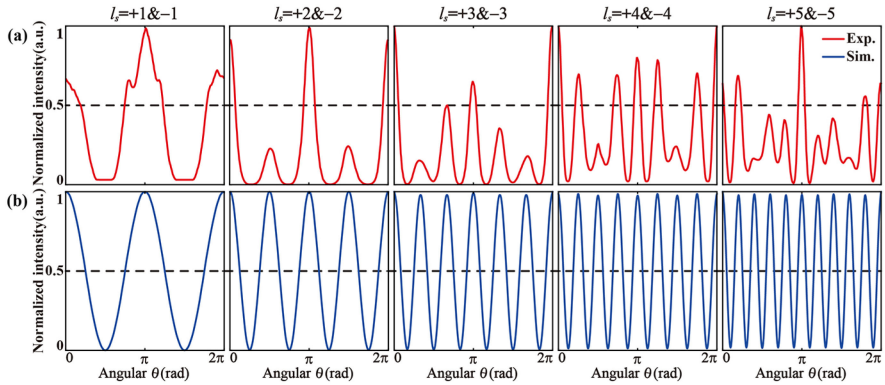

Fig. 4. (a) Experimental and (b) simulated ring intensity curves along the angular direction.

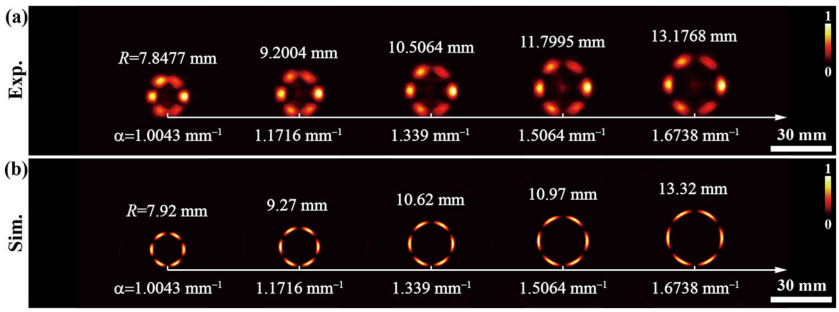

Fig. 5. (a) Experimental and (b) simulated intensity profiles of THz SPV beams with different radial wave vectors.

is also a ring with equally spaced breakpoints. Moreover, the ring radius is the same as the superimposed topological charge changes. The experiments match well with simulations. Therefore, both experimental and simulated results confirm the perfect vortex property of the THz SPV beams.

It is worth noting that the ring profile of THz SPV beams is split by some breakpoints and the number of breakpoints is equal to $2|l|$. Thus, the superimposed topological charge carried by these THz PV beams can be determined by measuring the number of breakpoints. According to the normalized intensity patterns of THz SPV beams, the normalized intensity curves along the angular direction are plotted. Figs. 4(a) and 4(b) show the experimental and simulated curves, respectively. The detailed data processing is as follows: using coordinate transformation, an intensity pattern is transformed from Cartesian coordinates (x,y) to polar coordinates (r,θ). In such a situation, the ring is straightened in polar coordinates. Along with the straightened ring, a ring intensity curve along the angular direction is plotted. The minimum of the curve less than a certain value (e.g., less than 0.5, the position of the dotted line in Fig. 4) is considered as a valid valley. The location of these valleys corresponds to the breakpoint of the ring. The number of valleys obtained by this data processing is consistent with the number of breakpoints. The effectiveness of this data processing is confirmed by the experimental and simulated curves. In addition, some other methods can be introduced to identify such vortex patterns with superposition states, such as the artificial neural network [28]. Therefore, the superimposed topological charge of the THz SPV beams can be determined by its intensity patterns rather than detected by a device. This property can simplify the transmission system of THz SPV beams.

To obtain THz SPV beam with various sizes, the variation of ring radius with radial wave vector is investigated. We generated THz SPV beams with different radial wave vectors in the experiment. Fig. 5(a) shows the normalized intensity profiles. For the SOPEs, the superimposed topological charge $l_s = +1\&{-}1$, the radial wave vector ranges from $\alpha = 1.0043\ \text{mm}^{-1}$ to $\alpha = 1.6738\ \text{mm}^{-1}$. As the radial wave vector increases, the ring radius becomes larger, but the number of breakpoints remains the same. Meanwhile, the ring radius of THz SPV beams is computed by fitting the intensity profile. The fitting formula for the intensity profiles is the same as the previous one. The fitted ring radius is marked in the intensity patterns. In the experiment, the fitting relationship between the ring radius R (units: mm) and radial wave vector α (units: mm^{-1}) can be expressed as a linear function: $R = -0.10{+}7.92\alpha$, whose correlation coefficient up to 0.99986. This indicates that the ring radius is almost positively linearly related to the radial wave vector. Along with the same experimental parameters, the numerically simulated results based on the angular spectrum are shown in Fig. 5(b). In the simulation, the fitting relationship between the ring radius R (units: mm) and radial wave vector α (units: mm^{-1}) can be expressed as a linear function: $R = -0.18{+}8.07\alpha$, whose correlation coefficient is 1. This indicates that the ring radius is positively linearly related

to the radial wave vector. The experimental function is very closely related to the numerically simulated one. Therefore, the ring radius of THz SPV beams is controllable. By controlling the radial wave vector, the THz SPV beam with any desired ring radius can be obtained.

V. Conclusion

In summary, we generated the THz SPV beams by using the designed SOPEs at 0.3 THz. The designed SOPEs are simple and easy to fabricate, whose phase mainly contains two values. The intensity profile of THz SPV beams is a ring with equally spaced breakpoints. The superimposed topological charge carried by the THz SPV beams is directly judged by identifying the number of breakpoints. The transmission system of THz SPV beams can be simplified. As the superimposed topological charge changes, the ring radius of THz SPV beams remains almost constant in the experiment. The relative error of the maximum and minimum of the ring radius is only 0.96%, which is very small. A small relative error will increase the coupling efficiency of the fiber communication systems based on THz SPV beams. The ring radius of THz SPV beams varies with the radial wave vector, which can be expressed as a linear function. The correlation coefficient up to 0.99986 in the experiment. This means that the ring radius of THz PV beams is controllable. It is possible to obtain a THz SPV beam with any desired ring radius by adjusting the radial wave vector. The experimental results are in good agreement with the numerically simulated ones. This work can couple the THz SPV beams with multiple superimposed topological charges into a fiber with fixed radius, which has promising applications for THz fiber communication systems based on vortex beams.

References

[1] Z. Chen *et al.*, "A survey on terahertz communications," *China Commun.*, vol. 16, no. 2, pp. 1–35, 2019.

[2] T. Nagatsuma, G. Ducournau, and C. C. Renaud, "Advances in terahertz communications accelerated by photonics," *Nature Photon.*, vol. 10, pp. 371–379, 2016.

[3] A. M. Yao, and M. J. Padgett, "Orbital angular momentum: Origins, behavior and applications," *Adv. Opt. Photon.*, vol. 3, no. 2, pp. 161–204, 2011.

[4] J. Wang *et al.*, "Terabit free-space data transmission employing orbital angular momentum multiplexing," *Nature Photon.*, vol. 6, pp. 488–496, 2012.

[5] N. Bozinovic *et al.*, "Terabit-scale orbital angular momentum mode division multiplexing in fibers," *Science*, vol. 340, no. 6140, pp. 1545–1548, 2013.

[6] Z. Xie *et al.*, "Integrated (de)multiplexer for orbital angular momentum fiber communication," *Photon. Res.*, vol. 6, no. 7, pp. 743–749, 2018.

[7] L. Allen, M. W. Beijersbergen, R. J. C. Spreeuw, and J. P. Woerdman, "Orbital angular momentum of light and the transformation of Laguerre-Gaussian laser modes," *Phys. Rev. A*, vol. 45, no. 11, pp. 8185–8189, 1992.

[8] H. Zhao, B. Quan, X. Wang, C. Gu, J. Li, and Y. Zhang, "Demonstration of orbital angular momentum multiplexing and demultiplexing based on a metasurface in the terahertz band," *ACS Photon.*, vol. 5, no. 5, pp. 1726–1732, 2018.

[9] H. Li *et al.*, "Guiding terahertz orbital angular momentum beams in multi-mode kagome hollow-core fibers," *Opt. Lett.*, vol. 42, no. 2, pp. 179–182, 2017.

[10] N. Aflakian, T. P. LaFave, K. O. Kenneth, S. Ashrafi, and D. L. MacFarlane, "Design, fabrication, and demonstration of a dielectric vortex waveguide in the sub-terahertz region," *Appl. Opt.*, vol. 56, no. 25, pp. 7123–7129, 2017.

[11] V. Sharif, and H. Pakarzadeh, "Terahertz hollow-core optical fibers for efficient transmission of orbital angular momentum modes," *J. Lightw. Technol.*, vol. 39, no. 13, pp. 4462–4468, 2021.

[12] A. S. Ostrovsky, C. Rickenstorff-Parrao, and V. Arrizón, "Generation of the 'perfect' optical vortex using a liquid-crystal spatial light modulator," *Opt. Lett.*, vol. 38, no. 4, pp. 534–536, 2013.

[13] M. Chen, M. Mazilu, Y. Arita, E. M. Wright, and K. Dholakia, "Dynamics of microparticles trapped in a perfect vortex beam," *Opt. Lett.*, vol. 38, no. 22, pp. 4919–4922, 2013.

[14] M. Khodadadi Karahroudi, S. A. Moosavi, A. Mobashery, B. Parmoon, and H. Saghafifar, "Performance evaluation of perfect optical vortices transmission in an underwater optical communication system," *Appl. Opt.*, vol. 57, no. 30, pp. 9148–9154, 2018.

[15] D. Deng, Y. Li, H. Zhao, Y. Han, J. Ye, and S. Qu, "High-capacity spatial-division multiplexing with orbital angular momentum based on multi-ring fiber," *J. Opt.*, vol. 21, no. 5, 2019, Art. no. 055601.

[16] M. V. Jabir, N. Apurv Chaitanya, A. Aadhi, and G. K. Samanta, "Generation of 'perfect' vortex of variable size and its effect in angular spectrum of the down-converted photons," *Sci. Rep.*, vol. 6, no. 1, 2016, Art. no. 21877.

[17] P. Vaity, and L. Rusch, "Perfect vortex beam: Fourier transformation of a bessel beam," *Opt. Lett.*, vol. 40, no. 4, pp. 597–600, 2015.

[18] Y. Yang, X. Ye, L. Niu, K. Wang, Z. Yang, and J. Liu, "Generating terahertz perfect optical vortex beams by diffractive elements," *Opt. Exp.*, vol. 28, no. 2, pp. 1417–1425, 2020.

[19] V. V. Kotlyar, A. A. Kovalev, and A. P. Porfirev, "Optimal phase element for generating a perfect optical vortex," *J. Opt. Soc. Amer. A*, vol. 33, no. 12, pp. 2376–2384, 2016.

[20] X. Wei *et al.*, "Generation of arbitrary order bessel beams via 3D printed axicons at the terahertz frequency range," *Appl. Opt.*, vol. 54, no. 36, pp. 10641–10649, 2015.

[21] Y. Yang, L. Niu, Z. Yang, and J. Liu, "Measuring the topological charge of terahertz vortex beams with a focal hyperbolic lens," *Appl. Opt.*, vol. 59, no. 15, pp. 4685–4691, 2020.

[22] Q. Cao, and J. Jahns, "Comprehensive focusing analysis of various fresnel zone plates," *J. Opt. Soc. Amer. A*, vol. 21, no. 4, pp. 561–571, 2004.

[23] P. Schemmel, G. Pisano, and B. Maffei, "Modular spiral phase plate design for orbital angular momentum generation at millimetre wavelengths," *Opt. Exp.*, vol. 22, no. 12, pp. 14712–14726, 2014.

[24] C. Liu, L. Niu, K. Wang, and J. Liu, "3D-printed diffractive elements induced accelerating terahertz Airy beam," *Opt. Exp.*, vol. 24, no. 25, pp. 29342–29348, 2016.

[25] C. Liu, J. Liu, L. Niu, X. Wei, K. Wang, and Z. Yang, "Terahertz circular airy vortex beams," *Sci. Rep.*, vol. 7, no. 1, 2017, Art. no. 3891.

[26] Z.-X. Shen *et al.*, "Planar terahertz photonics mediated by liquid crystal polymers," *Adv. Opt. Mater.*, vol. 8, no. 7, 2020, Art. no. 1902124.

[27] J. W. Goodman, *Introduction to Fourier Optics*. New York, NY, USA: McGraw-Hill, 2005.

[28] M. Krenn *et al.*, "Twisted light transmission over 143 km," *Proc. Nature Acad. Sci.*, vol. 113, no. 48, 2016, Art. no. 13648.